# Biophysics-based data assimilation of longitudinal tau and amyloid-$\beta$ PET scans

Zheyu Wen[1], Ali Ghafouri[1], and George Biros[1]

Oden Institute, University of Texas at Austin, 201 E. 24th Street, Austin, Texas, USA
{zheyw,ghafouri}@utexas.edu, biros@oden.utexas.edu

**Abstract.** Misfolded tau and amyloid-$\beta$ (A$\beta$) are hallmark proteins of Alzheimer's Disease (AD). Due to their clinical significance, rich datasets that track their temporal evolution have been created. For example, ADNI has hundreds of subjects with PET imaging of both these two proteins. Interpreting and combining this data beyond statistical correlations remains a challenge. Biophysical models offer a complementary avenue to *assimilating* such complex data and eventually helping us better understand disease progression. To this end, we introduce a mathematical model that tracks the dynamics of four species (normal and abnormal tau and A$\beta$) and uses a graph to approximate their spatial coupling. The graph nodes represent gray matter regions of interest (ROI), and the edges represent tractography-based connectivity between ROIs. We model interspecies interactions, migration, proliferation, and clearance. Our biophysical model has seven unknown scalar parameters plus unknown initial conditions for tau and A$\beta$. Using imaging scans, we can calibrate these parameters by solving an inverse problem. The scans comprise longitudinal tau and A$\beta$ PET scans, along with MRI for subject-specific anatomy. We propose an inversion algorithm that stably reconstructs the unknown parameters. We verify and test its numerical stability in the presence of noise using synthetic data. We discovered that the inversion is more stable when using multiple scans. Finally, we apply the overall methodology on 334 subjects from the ADNI dataset and compare it to a commonly used tau-only model calibrated by a single PET scan. We report the $R^2$ and relative fitting error metrics. The proposed method achieves $R^2 = 0.82$ compared to $R^2 = 0.64$ of the tau-only single-scan reconstruction.

**Keywords:** Tau propagation · Amyloid-$\beta$ · Inverse problem.

## 1 Introduction

Tau inclusions and amyloid-$\beta$ plagues characterize Alzheimer's disease [1–5]. Longitudinal Tau-PET and A$\beta$-PET scans [9] and other biomarkers suggest strong correlations between the two proteins. It is believed that A$\beta$ accelerates misfolded tau aggregation [6–8]. Here we introduce a phenomenological mathematical model and propose a method to assimilate it with longitudinal PET scans. The model allows us to systematically integrate subject-specific clinical information and

explore spatio-temporal patterns using only a handful of parameters. In Figure 1 we summarize the main components of our approach.

*Contributions:* **(i)** We introduce a coupled tau-A$\beta$ biophysical model, which is a system of coupled ordinary differential equations. **(ii)** We present a gradient-based inversion algorithm to assimilate the model with longitudinal Tau-PET and A$\beta$-PET scans. **(iii)** We investigate the invertibility, forecast skill of the inversion scheme using synthetic data. We found that using multiple scans leads to a more stable inverse problem. **(iv)** We evaluate the proposed model on data from 334 subjects from the ADNI clinical dataset [20]. We found that the multi-scan assimilated coupled problem improves significantly the state of the art.

*Related work:* There are numerous works that use machine learning to integrate all the subject-specific data, e.g. [10,11] and the references therein. There are also several works that quantify the cumulative tau/A$\beta$ abnormality using interpolation/signal processing techniques [12–15,35]. Our approach is motivated by the temporal-ordering abnormal tau and discussion in those studies. Model-driven assimilation of longitudinal multimodal scans in the context of AD while accounting for the coupled interactions between tau and A$\beta$ is a novel approach, to our knowledge. The graph-based approximation of spatial spreading was introduced in [18, 19] and has been used by many groups. Tau-only biophysical models include the Fisher-Kolmogorov (FK) and the Heterodimer Fisher-Kolmogorov (HFK) models [25,33,34], and are typically calibrated using one scan. In a recent study [22] uses machine learning on tau/A$\beta$ data to stratify subjects and to fit different tau-models to different subject cohorts using a tau-only model.

## 2 Methodology

Our model leverages several previous works on assimilating tau-only models [24–26, 33, 34] with medical images. The basic idea is to model the per-ROI aggregate evolution of tau/A$\beta$ and use the ROI graph structure to capture spatial-dependencies. Using diffusion weighted images we can extract the connectivity between $N$ different ROIs with adjacency matrix $\mathbf{D}$. We follow the exact same method described in [33], but any other method can be used for this purpose. Given $\mathbf{D}$, we define the graph Laplacian $\mathbf{L} = \text{diag} \sum_{j=1,j\neq i}^{N} [\mathbf{D}(\mathbf{w})]_{ij} - \mathbf{D}(\mathbf{w})$ [27] to model spatial spreading of abnormal tau and A$\beta$.

For each ROI (graph node), we track the time evolution of four species: the abnormal tau and A$\beta$, $c_a(t)$ and $b_a(t)$ respectively; and the normal tau and A$\beta$, $c_n(t)$ and $b_n(t)$ respectively. Here $t$ represents time from the onset of the disease, the *disease age*. We remark that $t$ is unknown. We discuss a way to address this further below. We use the boldface $\mathbf{c}_a(t)$ and $\mathbf{b}_a(t)$ to indicate the vector values for all ROIs and use a similar notation for A$\beta$. Both normal and abnormal scores are normalized to $[0, 1]$. Next we describe how we define them.

First, we preprocess the Tau-PET and A$\beta$ as shown in Figure 1**(A)**. For each subject, we map the chronologically first T1 MRI to the parcellated MUSE atlas [29] using FSL [37] and define the subject-specific ROIs. Then, Tau-PET

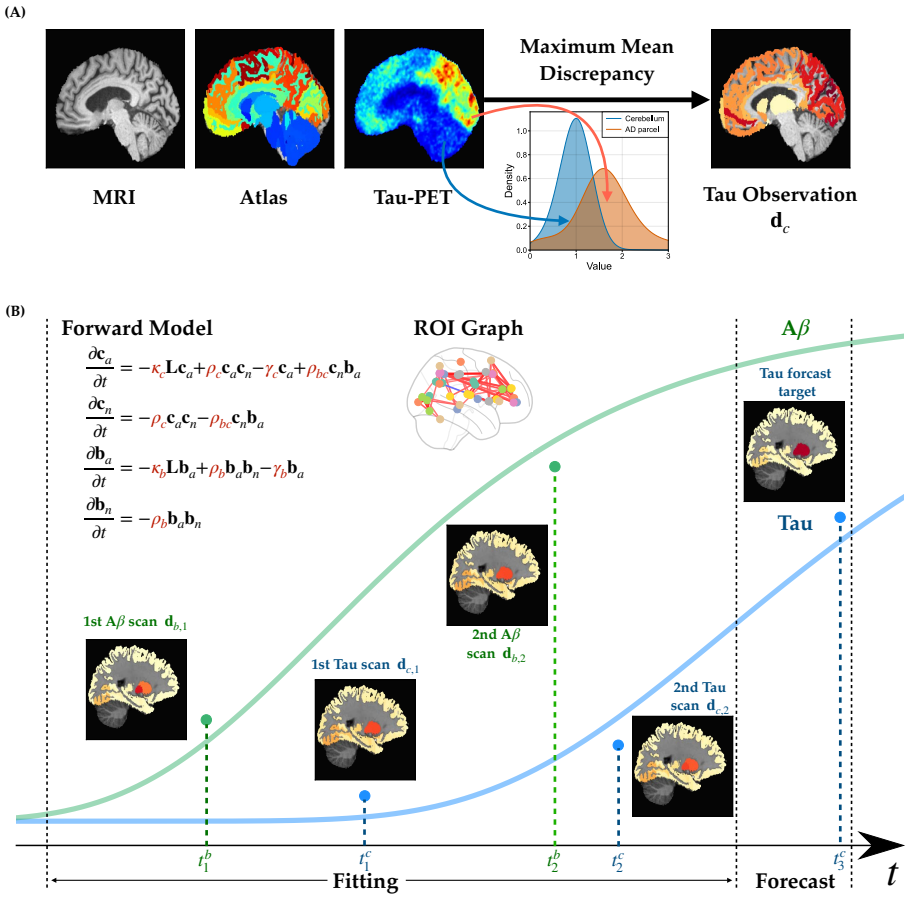


Fig. 1: Summary of the overall approach. **(A)** Data preprocessing to generate the data for the model calibration. Given a parcellated atlas and the subject MRI, we parcellate the subject image into atlas-defined ROIs using image registration. Following [33], we use the Maximum Mean Discrepancy (MMD) score to quantify the distributional distance between an ROI and the cerebellum tau/A$\beta$. **(B)** Our objective is to fit an ODE model to observed tau / A$\beta$ MMDs. We use an auxiliary disease-age model to define the time $t$ of the observed Tau-PET / A$\beta$-PET scans. Here $t_1^c$ indicates the first tau PET scan in disease-age $t$, defined in Section 2. $t_2^c$ indicates the second tau PET scan. Similarly $t_1^b$ and $t_2^b$ define the time of A$\beta$ scans. Once the mathematical is calibrated or assimilated with the scans we could used to forecast future tau scores and disease progression.

and A$\beta$-PET data are normalized by the median value of the tau uptake in the cerebellum. We define ROI abnormality scores as follows: By viewing voxelwise tau values as samples from a distribution, we use the maximum mean discrepancy

(MMD) [30] metric to define a distance between the tau/A$\beta$ distribution of the ROI and the cerebellum. Let $\mu_{c,i}$ denote the Tau MMD for the $i_{\text{th}}$ parcel. Then the abnormality score is given by by $d_c^i = 1 - e^{-\mu_{c,i}\sigma}$, where $d_c^i$ is tau observation at the $i^{\text{th}}$ parcel in the graph, and $\sigma = 0.3$ is a hyperparameter. Similarly, we define $\mu_{b,i}$ and $d_b^i$ for A$\beta$. Normal protein scores are also defined to be in $[0, 1]$ but they are not observable in the data.

The first challenge is that in order to define our ODE solution we need initial conditions and the time since the disease onset, the so called *"disease age"*—which is unknown. Several groups have proposed methods to estimate it. We use the work from [35] in which the authors propose a Disease Progression Score (DPS) that extracts a disease ages from scans. For each subject $i$, the disease age for scan $j$, is denoted by $t_{ij}$ and is assumed to be given by $t_{ij} = a_i \mathtt{t}_{ij} + b_i$, where $\mathtt{t}_{ij}$ is the actual chronological time of scan $j$. Then the disease age is mapped to a global, per subject, tau abnormality score using a logistic function with common parameters for all subjects. Then logistic regression is used to determine the age-to-tau parameters as well as the $a_i, b_i$ for each subject $i$. Then $t_{ij}$ is normalized by using a shifted sigmoid function where the shift is the cohort mean age. This normalized value indicates the disease age $t$ and is the time variable used in our ODE model. We remark that this normalization is critical since absolute chronological times are meaningless.

A natural question is why not using the first scan and then defining $t$ as the relative time based on the first scan. This approach was tested for tau-only models in [21,33,34] and it does not work because the observational time horizon is too short to stably reconstruct the dynamics of disease progression.

**Tau-A$\beta$ HFK Model:** The Tau-A$\beta$ HFK is given by the equation below with $\mathbf{c}_a(t), \mathbf{c}_n(t), \mathbf{b}_a(t), \mathbf{b}_n(t) \in \mathbb{R}_+^N \times (0, T]$:

$$\text{Abnormal tau:} \quad \frac{\partial \mathbf{c}_a}{\partial t} = -\kappa_c \mathbf{L}\mathbf{c}_a + \rho_c \mathbf{c}_a \mathbf{c}_n - \gamma_c \mathbf{c}_a + \rho_{bc} \mathbf{c}_n \mathbf{b}_a, \tag{1a}$$

$$\text{Normal tau:} \quad \frac{\partial \mathbf{c}_n}{\partial t} = -\rho_c \mathbf{c}_a \mathbf{c}_n - \rho_{bc} \mathbf{c}_n \mathbf{b}_a, \tag{1b}$$

$$\text{Abnormal A}\beta\text{:} \quad \frac{\partial \mathbf{b}_a}{\partial t} = -\kappa_b \mathbf{L}\mathbf{b}_a + \rho_b \mathbf{b}_a \mathbf{b}_n - \gamma_b \mathbf{b}_a, \tag{1c}$$

$$\text{Normal A}\beta\text{:} \quad \frac{\partial \mathbf{b}_n}{\partial t} = -\rho_b \mathbf{b}_a \mathbf{b}_n. \tag{1d}$$

The initial conditions (IC) are given $\mathbf{c}_a(0) = \mathbf{p}_c$, $\mathbf{c}_n(0) = \mathbf{1} - \mathbf{p}_c$, $\mathbf{b}_a(0) = \mathbf{p}_b$ and $\mathbf{b}_n(0) = \mathbf{1} - \mathbf{p}_b$, which are parameterized by $\mathbf{p}_c$ and $\mathbf{p}_b$. Equation (1) defines the following mechanism: The abnormal tau $\mathbf{c}_a$ spreads from the IC regions to the whole graph due to $\mathbf{L}$ scaled by diffusivity constant $\kappa_c \in \mathbb{R}_+$. Abnormal tau causes the transition of normal $\mathbf{c}_n$ into abnormal via the $\rho_c \mathbf{c}_a \mathbf{c}_n$ and $\rho_c \in \mathbb{R}_+$. We also account for clearance of abnormal tau $\mathbf{c}_a$ using the $-\gamma_c \mathbf{c}_a$ and $\gamma_c \in \mathbb{R}_+$. We assume that abnormal A$\beta$ catalyzes tau growth [7,8,25] and represent this by combining A$\beta$ with healthy tau in the term $\rho_{bc} \mathbf{c}_n \mathbf{b}_a$ where $\rho_{bc} \in \mathbb{R}_+$, and normal tau decreases by subtracting the corresponding amount. We describe propagation

of A$\beta$ similarly with parameters $\kappa_b$, $\rho_b$ and $\gamma_b \in \mathbb{R}_+$ The ODE model is defined for $t \in (0, T]$.

**Data assimilation:** We define an inverse problem using the following subject-specific objective function:

$$\mathcal{J} = \frac{1}{s_c}\sum_{i}^{s_c} \|\mathbf{c}_a(t_i^c) - \mathbf{d}_{c,i}\|_2^2 + \frac{1}{s_b}\sum_{i}^{s_b} \left\|\mathbf{b}_a(t_i^b) - \mathbf{d}_{b,i}\right\|_2^2 + \lambda_1 \log(1-\mathbf{p}_c) + \lambda_2 \log(1-\mathbf{p}_b).$$

where $\mathbf{d}_{c,i}$ and $\mathbf{d}_{b,i}$ are the $i^{\text{th}}$ PET-derived tau and A$\beta$ ROI MMD scores. $\mathbf{c}_a(t_i^c)$ and $\mathbf{b}_a(t_i^b)$ is the ODE solution at $t = t_i^c$ and $t = t_i^b$. The regularization parameters $\lambda_1 > 0$ and $\lambda_2 > 0$ ensure that $\boldsymbol{\theta}_p < \mathbf{1}$ elementwise. To further regularize the reconstruction of the initial conditions and assuming that the abnormal proteins originate in specific locations, we introduce the sparsity constraints for $\mathbf{p}_c$ and $\mathbf{p}_b$: $\|\mathbf{p}_c\|_0 = s^{\max,c}$ and $\|\mathbf{p}_b\|_0 = s^{\max,b}$ where $\|\mathbf{z}\|_0$ counts the number of non-zeros of input vector $\mathbf{z}$. $s^{\max,c}$ and $s^{\max,b}$ are two constants. We define $\boldsymbol{\theta}_7 := \{\kappa_c, \rho_c, \gamma_c, \rho_{bc}, \kappa_b, \rho_b, \gamma_b\} \in \mathbb{R}^7$ and $\boldsymbol{\theta}_p := \{\mathbf{p}_c, \mathbf{p}_b\} \in \mathbb{R}^{2N}$. Then the unknown parameters are $\boldsymbol{\theta} := \{\boldsymbol{\theta}_7, \boldsymbol{\theta}_p\} \in \mathbb{R}^{7+2N}$ comprising scalar ODE coefficients and the initial conditions for the abnormal proteins.

Then the inverse problem is defined as follows:

$$\begin{aligned} &\min_{\boldsymbol{\theta}>\mathbf{0}} \mathcal{J}(\boldsymbol{\theta}) \text{ subject to:} \\ &\qquad \text{Equation (1) holds and } \|\mathbf{p}_c\|_0 = s^{\max,c},\ \|\mathbf{p}_b\|_0 = s^{\max,b}. \end{aligned} \tag{2}$$

Here $\mathcal{J}$ is an implicit function of $\boldsymbol{\theta}$ through the solution of Equation (1). We use a gradient/adjoint-based method [38] to solve Equation (2). Let $\mathcal{L}$ denote the Lagrangian and $\boldsymbol{\alpha}_{ca}$, $\boldsymbol{\alpha}_{cn}$, $\boldsymbol{\alpha}_{ba}$, and $\boldsymbol{\alpha}_{bn}$ adjoint variables for $\mathbf{c}_a$, $\mathbf{c}_n$, $\mathbf{b}_a$ and $\mathbf{b}_n$ respectively. The adjoint equation is given

$$\frac{\partial \boldsymbol{\alpha}_{ca}}{\partial t} = \kappa_c \mathbf{L}^\intercal \boldsymbol{\alpha}_{ca} + \rho_c \mathbf{c}_n(\boldsymbol{\alpha}_{cn} - \boldsymbol{\alpha}_{ca}) + \gamma_c \boldsymbol{\alpha}_{ca} + \xi_{ca}, \tag{3a}$$

$$\frac{\partial \boldsymbol{\alpha}_{cn}}{\partial t} = (\rho_c \mathbf{c}_a + \rho_{bc}\mathbf{b}_a)(\boldsymbol{\alpha}_{cn} - \boldsymbol{\alpha}_{ca}), \tag{3b}$$

$$\frac{\partial \boldsymbol{\alpha}_{ba}}{\partial t} = \kappa_b \mathbf{L}^\intercal \boldsymbol{\alpha}_{ba} + \rho_b \mathbf{b}_n(\boldsymbol{\alpha}_{bn} - \boldsymbol{\alpha}_{ba}) + \gamma_b \boldsymbol{\alpha}_{ba} + \rho_{bc}\mathbf{c}_n(\boldsymbol{\alpha}_{cn} - \boldsymbol{\alpha}_{ca}) + \xi_{ba}, \tag{3c}$$

$$\frac{\partial \boldsymbol{\alpha}_{bn}}{\partial t} = \rho_b \mathbf{b}_a(\boldsymbol{\alpha}_{bn} - \boldsymbol{\alpha}_{ba}), \tag{3d}$$

$$\boldsymbol{\alpha}_{ca}(T) = \begin{cases} \mathbf{d}_{c,s_c} - \mathbf{c}_a(t_{s_c}^c) & \text{if } t_{s_c}^c = T \\ \mathbf{0} & \text{otherwise} \end{cases}, \tag{3e}$$

$$\boldsymbol{\alpha}_{ba}(T) = \begin{cases} \mathbf{d}_{b,s_b} - \mathbf{b}_a(t_{s_b}^b) & \text{if } t_{s_b}^b = T \\ \mathbf{0} & \text{otherwise} \end{cases}, \tag{3f}$$

where $\mathbf{L}^\intercal$ denotes matrix transpose of $\mathbf{L}$, $\xi_{ca} = \frac{1}{s_c}\sum_i^{s_c}(\mathbf{c}_a(t) - \mathbf{d}_{c,j})\delta(t - t_i^c)(1 - \delta(t-T))$ and $\xi_{ba} = \frac{1}{s_b}\sum_i^{s_b}(\mathbf{b}_a(t) - \mathbf{d}_{b,j})\delta(t - t_i^b)(1 - \delta(t-T))$; where $\delta(0) = 1, \delta(x) = 0, \forall x \neq 0$. $\partial_{\boldsymbol{\theta}}\mathcal{J}$ is computed as follows: $\frac{\partial \mathcal{L}}{\partial \kappa_c} = \int \alpha_{ca}^\intercal \mathbf{L}\mathbf{c}_a dt$, $\frac{\partial \mathcal{L}}{\partial \rho_c} =$

$\int(\alpha_{cn}-\alpha_{ca})^\intercal(\mathbf{c}_a\mathbf{c}_n)dt$, $\frac{\partial\mathcal{L}}{\partial\gamma_c}=\int\alpha_{ca}^\intercal\mathbf{c}_a dt$, $\frac{\partial\mathcal{L}}{\partial\rho_{bc}}=\int(\alpha_{cn}-\alpha_{ca})^\intercal\mathbf{b}_a\mathbf{c}_n dt$, $\frac{\partial\mathcal{L}}{\partial\kappa_b}=\int\alpha_{ba}^\intercal\mathbf{L}\mathbf{b}_a dt$, $\frac{\partial\mathcal{L}}{\partial\rho_b}=\int(\alpha_{bn}-\alpha_{ba})^\intercal(\mathbf{b}_a\mathbf{b}_n)dt$, $\frac{\partial\mathcal{L}}{\partial\gamma_b}=\int\alpha_{ba}^\intercal\mathbf{b}_a dt$, $\frac{\partial\mathcal{L}}{\partial\mathbf{p}_c}=\alpha_{cn}-\alpha_{ca}+\frac{\lambda_1}{\mathbf{p}_c-1}$ and $\frac{\partial\mathcal{L}}{\partial\mathbf{p}_b}=\alpha_{bn}-\alpha_{ba}+\frac{\lambda_2}{\mathbf{p}_b-1}$. To update $\boldsymbol{\theta}$, we first solve Equation (1), and then solve Equation (3) backward in time, i.e., in $t\in[T,0]$; then given forward and adjoint trajectories we can compute $\partial_{\boldsymbol{\theta}}\mathcal{J}$ and use a gradient descent scheme. We use a quasi-Newton method and use the algorithm in [33] to handle sparsity constraints.

**Numerical discretization of forward and adjoint problem:** We use the LSODA ODE solver [36]. We use a limited memory quasi-Newton L-BFGS algorithm [28] to solve the optimization problem. We initialize $\boldsymbol{\theta}=\mathbf{0}$. The regularization parameters $\lambda_1$ and $\lambda_2$ is chosen to ensure $p_c<1$ and $p_b<1$. We set $s^{\max,c}=5$, $s^{\max,b}=10$. Further, we impose $\boldsymbol{\theta}_7\in[0,20]^7$.

## 3 Results

The proposed data assimilation scheme works with an arbitrary number of scans for each biomarker. We investigate four algorithmic variants categorized by (1) model structure: tau-only vs tau-A$\beta$, and (2) number of scans used in the reconstruction: single vs many. We term these variants as Tau-only Single Scan (short as Tau-1S), Tau-only Multiple Scans (Tau-MS), Tau-A$\beta$ Single Scan (TauA$\beta$-1S) or Tau-A$\beta$ Multiple Scans (TauA$\beta$-MS). We evaluate these variants using synthetic and clinical data. We seek to answer the following questions:

**(Q1)** Is the inversion scheme numerically accurate and stable? To answer this, we generate synthetic data using Equation (1), pollute them with artificial noise, and reconstruct the parameters $\boldsymbol{\theta}$ by solving Equation (2).
**(Q2)** What is the qualitative and quantitative performance in clinical data? To answer this, we evaluate the methods using subjects from the ADNI dataset.

**(Q1) Testing inversion algorithm:** We verified the ability of the inversion algorithm to reconstruct $\boldsymbol{\theta}$ in the absence of modeling errors using synthetically generated data. The observation data is generated by Equation (1) with specified $\boldsymbol{\theta}$. In particular we use initial conditions $\boldsymbol{\theta}_p$ with nonzero values at the entorhinal cortex, as it is typically done in biophysics-based simulations [25]. The ODE coefficients $\boldsymbol{\theta}_7$ are random. For the TauA$\beta$-1S and TauA$\beta$-MS assimilation scenarios we performed 100 synthetic inversions/scenario for which we report statistics. TauA$\beta$-1S uses a single tau (and a single A$\beta$) observation at $t=0.95$ while TauA$\beta$-MS uses four tau/A$\beta$ observations at $t=[0.8,0.85,0.9,0.95]$. Different noise levels (0%–30%) are added to the observations. Further, we test the *forecast skill* of the model at $t=1.0$ that is beyond the observational time horizon ($t=0.95$). We measure performance using $e_{\mathbf{d}}=\|\mathbf{c}_a-\mathbf{d}_c\|_2/\|\mathbf{d}_c\|_2$. We report the results of this experiment in Figure 2(A). We conclude that using more scans results in more accurate and more stable, in the presence of noise, results both in assimilating observed data, but also in forecasting disease progression.

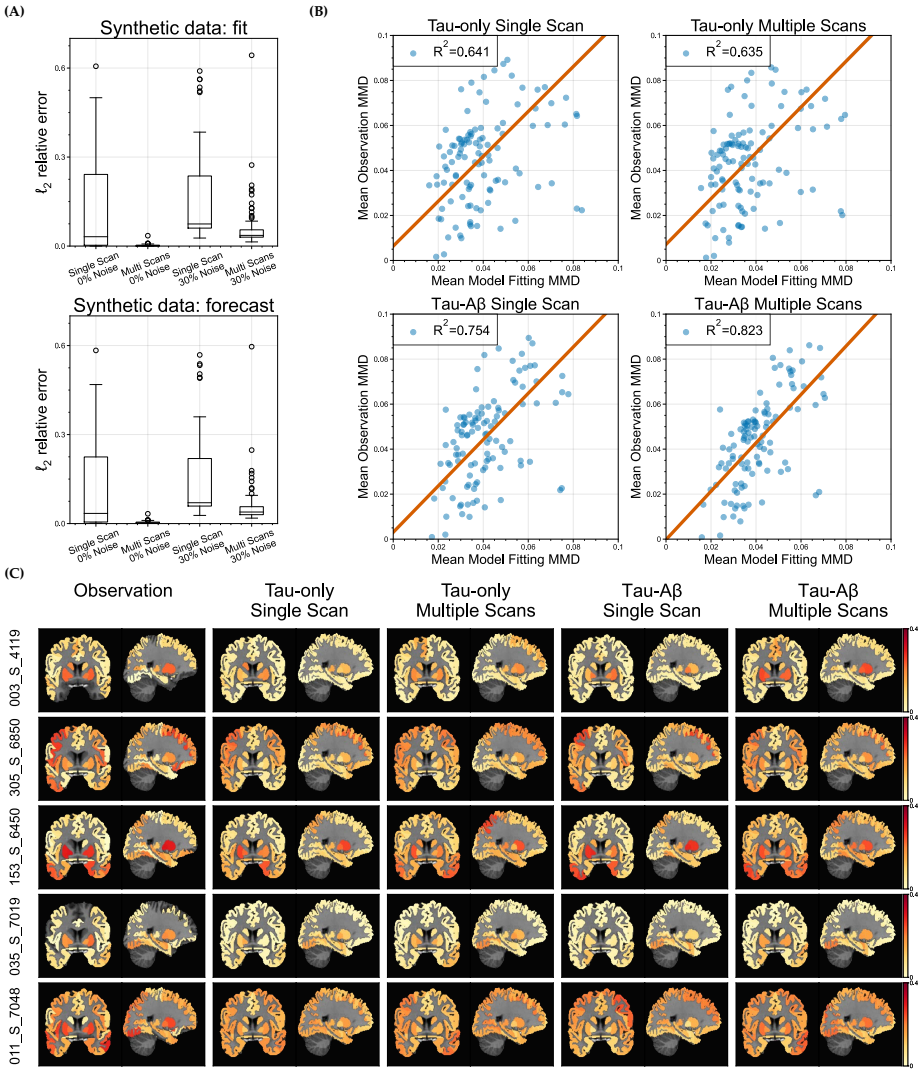


Fig. 2: **(A)** Synthetic inversion. We generate observations from tau-A$\beta$ HFK model with random parameters. Single observation takes at $t = 0.95$, while multiple observations take from $t = [0.8, 0.85, 0.9, 0.95]$. Prediction is set at $t = 1$. **(B)** Clinical inversion. We report the $R^2$ score for four assimilation scenarios applied on 334 ADNI subjects. Each dot in the scatter plot corresponds to a specific ROI for which, after assimilation, we average the scan MMD / model MMD across the subjects, and compute the $R^2$ value. The red line represents a fitted affine function to the scatters. **(C)** Visualization of inversion. We select five subjects with largest total abnormal tau (sum over ROIs). We report results for one CN subject, two MCI, and two AD subjects. From left to right, we show the observation data and results from the four assimilation scenarios.

Table 1: Performance in different Alzheimer's groups. For each algorithm variant, we compute the subject-wise $R^2$. The first column of each method demonstrates what is the percentage of subjects performs the best under the algorithm variant. The second column of each method shows the averaged $R^2$ over subjects. Overall, the method using Tau-A$\beta$ Multiple scans performs the best.

| Group | Tau-only Single Scan | | Tau-only Multiple Scans | | Tau-A$\beta$ Single Scan | | Tau-A$\beta$ Multiple Scans | |
|---|---|---|---|---|---|---|---|---|
| | % win | $R^2$ | % win | $R^2$ | % win | $R^2$ | % win | $R^2$ |
| CN | 0 | 4.70E−1 | 1.05 | 4.55E−1 | 20.52 | 5.81E−1 | **78.42** | **6.55E−1** |
| MCI | 1.59 | 4.86E−1 | 4.76 | 4.86E−1 | 14.28 | 5.65E−1 | **79.37** | **6.61E−1** |
| AD | 5.56 | 4.72E−1 | 0 | 4.73E−1 | 33.33 | 5.14E−1 | **61.11** | **6.14E−1** |

**(Q2) Clinical results:** We use MRI, Tau-PET, and Amyloid beta PET data from ADNI dataset [20]. We have 334 subjects that have both Tau-PET and A$\beta$-PET images (168 female and 166 male). The age mean(std) is 72.29(7.24). The acquisition time spans from 10/24/2005 to 01/12/2023. There are 190 Cognitive Normal (CN), 126 Mild Cognitive Impairment (MCI) and 18 Alzheimer's Disease (AD). The data was prepared using the workflow described in Section 2.

We evaluate the four different assimilation scenarios using $R^2(\mathbf{d}, \mathbf{c}) = \frac{\sum_i (d_i - c_i)^2}{\sum_i (d_i - \bar{d})^2}$, where $\bar{d}$ is the mean of entries of $\mathbf{d}$. The higher the $R^2$, the better the model fits the data. We present the population level $R^2$ for four algorithm variants in Fig. Figure 2(B). For each algorithm, we run the inversion for all 334 subjects and reconstruct $\boldsymbol{\theta}$ and the corresponding $\mathbf{c}_a(t)$. We average the model results across the subjects and obtain $\bar{\mathbf{c}}_a$. We repeat the same process for observations and obtain $\bar{\mathbf{d}}_c$. The population $R^2$ is computed Using $\bar{\mathbf{c}}_a$ and $\bar{\mathbf{d}}_c$. Overall, TauA$\beta$-MS, i.e., using a strongly coupled model and multiple scans, performs best. Notice that the Tau-1S model, as presented in [33], demonstrates superior performance compared to the model in [22, 25]. We further investigate the forecast ability of the proposed algorithms for the same subjects. In this experiment, the last tau scan is removed from the data used during assimilation. The $R^2$ figures are in the supplementary and the conclusion remains the same: TauA$\beta$-MS performs best.

Finally, we report per-subject $R^2$. We compare the $R^2$ values obtained with the different methods and compare them in Table Table 1. TauA$\beta$-MS "wins", i.e., has higher $R^2$ in 78.42% of the cases among CNs, 79.37% among MCIs, and 61.11% among AD subjects. In the same table, we also present the averaged $R^2$ over subjects within each group. Qualitatively, we evaluate five subjects from ADNI dataset in Figure 2(C). The first is a CN subject, followed by two MCI and two AD subjects. These are selected because they have the largest global tau in our cohort. We also present the quantitative evaluation of these five subjects in a table in the supplementary material.

## 4 Conclusions

We presented a Tau-A$\beta$ HFK model to simulate tau and amyloid-$\beta$ propagation in human brains. The inversion algorithm is proposed to estimate the operator

parameters and ICs in the model to fit clinical data. We test four algorithm variants. We find that the Tau-A$\beta$ model performs better than tau-only biophysical model. Also, using our synthetic experiments, we showed that given more observation scans, the inversion algorithm results in more accurate and more stable reconstructions. Qualitative and quantitative evaluation using ADNI subjects reaches similar conclusions. Our approach has also several limitations. Admittedly the coupled model is too simple to unveil the complex links between the tau and A$\beta$ dynamics. The model also does not include atrophy, which is a significant additional biomarker that is strongly correlated with tau aggregation. Importantly, the clinical significance of these preliminary results is to be seen. Our immediate plan is to check whether the model can help predict disease transition from CN to MCI or AD.

**Disclosure of Interests.** [1]

## References


1. Nisbet, Rebecca M., Juan P., Lars M. Ittner, and Jürgen Götz.: Tau aggregation and its interplay with amyloid-$\beta$. Acta neuropathologica **129**, 207–220 (2015)
2. Wang, L., et al.: Evaluation of tau imaging in staging Alzheimer disease and revealing interactions between $\beta$-amyloid and tauopathy. JAMA neurology **73**(9), 1070–1077 (2016)
3. Bloom, G. S.: Amyloid-$\beta$ and tau: the trigger and bullet in Alzheimer disease pathogenesis. JAMA neurology **71**(4), 505–508 (2014)
4. Ittner, L. M., and Götz, J.: Amyloid-$\beta$ and tau—a toxic pas de deux in Alzheimer's disease. Nature Reviews Neuroscience **12**(2), 67–72 (2011)
5. Hanseeuw, B.J., et al.: Association of amyloid and tau with cognition in preclinical Alzheimer disease: a longitudinal study. JAMA neurology **76**(8), 915–924 (2019)
6. Jack, C.R., et al.: Hypothetical model of dynamic biomarkers of the Alzheimer's pathological cascade. The Lancet Neurology **9**(1), 119–128 (2010)
7. Jack, C.R., et al.: Tracking pathophysiological processes in Alzheimer's disease: an updated hypothetical model of dynamic biomarkers. The lancet neurology **12**(2), 207–216 (2013)
8. Hampel, H., Cummings, J., Blennow, K., Gao, P., Jack Jr, C.R. and Vergallo, A.: Developing the ATX (N) classification for use across the Alzheimer disease continuum. Nature Reviews Neurology **17**(9), 580–589 (2021)
9. Johnson, K.A., et al.: Tau positron emission tomographic imaging in aging and early Alzheimer disease. Annals of neurology **79**(1), 110–119 (2016)
10. Young, Alexandra L., et al.: Uncovering the heterogeneity and temporal complexity of neurodegenerative diseases with Subtype and Stage Inference. Nature communications **9**(1), 4273 (2018)
11. Giorgio, J., Jagust, W. J., et al.: A robust and interpretable machine learning approach using multimodal biological data to predict future pathological tau accumulation. Nature communications **13**(1), 1887 (2022)


[1] The authors have no competing interests to declare that are relevant to the content of this article.

12. Baek, Min Seok, et al.: Temporal trajectories of in vivo tau and amyloid-$\beta$ accumulation in Alzheimer's disease. European journal of nuclear medicine and molecular imaging 47, 2879–2886 (2020)
13. Jagust, William J., and Susan M. Landau.: Temporal dynamics of $\beta$-amyloid accumulation in aging and Alzheimer disease. Neurology **9**(96) e1347–e1357 (2021)
14. Chen, Guangyu, et al.: Staging Alzheimer's disease risk by sequencing brain function and structure, cerebrospinal fluid, and cognition biomarkers. Journal of Alzheimer's Disease **3**(54), 983–993 (2016)
15. Veitch, Dallas P., et al.: Understanding disease progression and improving Alzheimer's disease clinical trials: Recent highlights from the Alzheimer's Disease Neuroimaging Initiative. Alzheimer's & Dementia **1**(15), 106–152 (2019)
16. H. Braak and K. Del Tredici.: The preclinical phase of the pathological process underlying sporadic alzheimer's disease. Brain **138**(10), 2814–2833 (2015)
17. H. Braak and E. Braak.: Neuropathological stageing of alzheimer-related changes. Acta neuropathologica **82**(4), 239–259 (1991)
18. Jucker, M. and Walker, L. C.: Self-propagation of pathogenic protein aggregates in neurodegenerative diseases. Nature **501**(7465), 45–51 (2013)
19. Iturria-Medina, Y., Sotero, et al.: Epidemic spreading model to characterize misfolded proteins propagation in aging and associated neurodegenerative disorders. PLoS computational biology **10**(11), e1003956 (2014)
20. Petersen, R.C., et al.: Alzheimer's disease neuroimaging initiative (ADNI): clinical characterization. Neurology **74**(3), 201–209 (2010) http://adni.loni.usc.edu/
21. K. Scheufele, S. Subramanian, and G. Biros.: Calibration of biophysical models for tau-protein spreading in alzheimer's disease from PET-MRI. arXiv preprint arXiv: 2007.01236 (2020)
22. Vogel, J.W., et al.: Four distinct trajectories of tau deposition identified in Alzheimer's disease. Nature medicine **27**(5), 871–881 (2021)
23. S. Fornari, A. Schäfer, M. Jucker, A. Goriely, and E. Kuhl.: Prion-like spreading of Alzheimer's disease within the brain's connectome. Journal of the Royal Society Interface **16**(159), 20190356 (2019)
24. Schäfer, A., Peirlinck, M., Linka, K., Kuhl, E., and Alzheimer's Disease Neuroimaging Initiative (ADNI).: Bayesian physics-based modeling of tau propagation in Alzheimer's disease. Frontiers in physiology 12, 702975 (2021)
25. Vogel, J. W., Iturria-Medina, et al.: Spread of pathological tau proteins through communicating neurons in human Alzheimer's disease. Nature communications **11**(1), 2612 (2020)
26. Kim, H. R., Lee, P., Seo, S. W., Roh, J. H., Oh, M., Oh, J. S., and Jeong, Y. Comparison of Amyloid beta and tau spread models in Alzheimer's disease. Cerebral Cortex **29**(10), 4291–4302 (2019)
27. Chung, F. R.: Spectral graph theory. American Mathematical Soc. Chapter 1 (1997)
28. Zhu, C., Byrd, R. H., Lu, P., and Nocedal, J.: Algorithm 778: L-BFGS-B: Fortran subroutines for large-scale bound-constrained optimization. ACM Transactions on mathematical software (TOMS) **23**(4), 550–560 (1997)
29. Doshi, J., Erus, G., Ou, Y., Resnick, S. M., Gur, R. C., Gur, R. E., and Alzheimer's Neuroimaging Initiative.: MUSE: MUlti-atlas region Segmentation utilizing Ensembles of registration algorithms and parameters, and locally optimal atlas selection. Neuroimage 127, 186–195 (2016)
30. Gretton, A., Borgwardt, K., Rasch, M. J., Schölkopf, B., and Smola, A.: A kernel two-sample test. The Journal of Machine Learning Research **13**(1), 723–773 (2012)

31. Dagley, A., LaPoint, M., Huijbers, W., Hedden, T., McLaren, D. G., Chatwal, J. P., and Schultz, A. P.: Harvard aging brain study: dataset and accessibility. Neuroimage 144, 255–258 (2017) https://habs.mgh.harvard.edu/
32. Tournier, J-Donald, et al.: MRtrix3: A fast, flexible and open software framework for medical image processing and visualisation. Neuroimage 202, 116–137 (2019)
33. Zheyu Wen, Ali Ghafouri, and George Biros. "A single-snapshot inverse solver for two-species graph model of tau pathology spreading in human Alzheimer disease." arXiv preprint arXiv:2402.06880 (2024)
34. Zheyu Wen, Ali Ghafouri, and George Biros.: A two-species model for abnormal tau dynamics in alzheimer's disease. International Conference on Medical Image Computing and Computer-Assisted Intervention. Cham: Springer Nature Switzerland (2023)
35. Ghazi, M.M. et al.: Robust parametric modeling of Alzheimer's disease progression. NeuroImage 225, 117460 (2021)
36. Petzold, Linda.: Automatic selection of methods for solving stiff and nonstiff systems of ordinary differential equations. SIAM journal on scientific and statistical computing **4**(1), 136–148 (1983)
37. Smith, S. M., Jenkinson, M., Woolrich, M. W., Beckmann, C. F., Behrens, T. E., Johansen-Berg, H., and Matthews, P. M.: Advances in functional and structural MR image analysis and implementation as FSL. Neuroimage 23, S208–S219 (2004)
38. Hinze, M. et al.: Optimization with PDE constraints . Springer Science & Business Media, (2008)